IL NUOVO CIMENTO Vol. 33 C, N. 4 Luglio-Agosto 2010
DOI 10.1393/ncc/i2010-10664-3

Colloquia: TOP2010

Bound-state effects in $t\bar{t}$ production at hadron colliders

H. Yokoya

Theory Unit, Physics Department, CERN - CH-1211 Geneva, Switzerland

(ricevuto il 16 Luglio 2010; approvato il 16 Luglio 2010; pubblicato online l'11 Ottobre 2010)

Summary. — We discuss the bound-state effects in $t\bar{t}$ production at hadron colliders. The effects can be sizable in the threshold region at the LHC, where $t\bar{t}$ pairs are predominantly produced via gluon-fusion process. The $t\bar{t}$ invariant-mass distribution as well as the top-quarks kinematical distributions are investigated. A prospect for the mass determination using the threshold events is discussed.

PACS 14.65.Ha – Top-quarks.
PACS 14.40.Pq – Heavy quarkonia.
PACS 12.38.-t – Quantum chromodynamics.

1. – Introduction

At the CERN Large Hadron Collider (LHC), $t\bar{t}$ pair-production is dominated by gluon-fusion process. The $t\bar{t}$ pair produced via gluon-fusion can be color-singlet or octet. Since the gluon distribution function is a rapidly decreasing function of its momentum fraction x, a substantial amount of the $t\bar{t}$ pair would be produced close to their mass threshold. Therefore, we would expect that contributions of the $t\bar{t}$ resonance can be sizable at the LHC. On the other hand, at the Tevatron, the main channel is $q\bar{q}$ annihilation, hence we anticipate that the resonance effects are not significant.

Since the discovery of the top-quark with its huge mass, $m_t \simeq 173\,\mathrm{GeV}$ [1], consequences of its expected large decay-width, $\Gamma_t \simeq 1.5\,\mathrm{GeV}$([1]), have been also considered seriously. Due to the large decay width, the $t\bar{t}$ bound states, sometimes called toponiums, cannot be formed individually [4], but they are merged into one broad resonance. This feature is observed by the fact that the binding energies of the bound states are the same order as the decay width; $E_B[^1S_0] \simeq 2\,\mathrm{GeV} \sim \Gamma_t$. To treat such a broad resonance formation, the Green's function formalism has been developed [5, 6]. Historically, it is mainly developed for the case of e^+e^- collisions [7], but only a few works can be found

([1]) Recent CDF and D0 measurements on the top-quark decay-width can be found in [2, 3].

in the study for hadron collisions [8]. Recently, with the above motivation facing the era of the LHC, the bound-state effects in $t\bar{t}$ production at hadron colliders have been studies in refs. [9-11]. In addition, inspired by these works or independently, there have also appeared studies concerning the bound-state formation in pair production of heavy colored particles which participate in models beyond the standard model [12-18]. In this report, we briefly explain the recent studies on the bound-state effects in $t\bar{t}$ production at hadron colliders [9-11].

2. – Bound-state effects at hadron colliders: $t\bar{t}$ invariant-mass distribution

In this section, we present a cross-section formalism for the $t\bar{t}$ invariant-mass distribution close to the $t\bar{t}$ threshold [9, 10]. It includes the all-order summation of Coulomb corrections via the non-relativistic framework which take into account the large decay-width of the top-quark, and also the effects of initial-state radiation (ISR) which is always significant at hadron colliders. The $t\bar{t}$ invariant-mass distribution at hadron colliders is written as

$$\frac{\mathrm{d}\sigma}{\mathrm{d}m_{t\bar{t}}}(s, m_{t\bar{t}}^2; i \to f) = \frac{2m_{t\bar{t}}}{s}\hat{\sigma}(m_{t\bar{t}}^2; i \to f) \times K_i^{(c)} \int_{\tau_0}^1 \frac{\mathrm{d}z}{z} F_i^{(c)}(z) \frac{\mathrm{d}\mathcal{L}_i}{\mathrm{d}\tau}\left(\frac{\tau_0}{z}\right), \tag{1}$$

where $\tau_0 = m_{t\bar{t}}^2/s$. We explain each term in turn. $\hat{\sigma}$ are the partonic cross-sections for various channels. As is well known, the S-wave parts of the cross-sections are most important in the threshold region. The leading S-wave contributions reside in the following channels: 1) $gg \to t\bar{t}\ [^1S_0^{[1]}]$; 2) $gg \to t\bar{t}\ [^1S_0^{[8]}]$; 3) $q\bar{q} \to t\bar{t}\ [^3S_1^{[8]}]$. For these channels, the bound-state effects are taken into account in the following manner:

$$\hat{\sigma}(s; i \to f) = [\hat{\sigma}(s; i \to f)]_{\mathrm{tree}} \times \frac{\mathrm{Im}\left[\widetilde{G}^{(c)}\left(E + i\Gamma_t, \vec{0}\right)\right]}{\mathrm{Im}\left[\widetilde{G}_0\left(E + i\Gamma_t, \vec{0}\right)\right]}, \tag{2}$$

where the non-relativistic Green's functions are defined by

$$\left[(E + i\Gamma_t) - \left\{-\frac{\nabla^2}{m_t} + V_{\mathrm{QCD}}^{(c)}(|\vec{r}|)\right\}\right] \widetilde{G}^{(c)}(E + i\Gamma_t, \vec{r}) = \delta^3(\vec{r}), \tag{3}$$

and $E = \sqrt{s} - 2m_t$ is the c.m. energy of the $t\bar{t}$ system measured from the threshold; $V_{\mathrm{QCD}}^{(c)}(r)$ is the QCD potential between the color-singlet ($c = 1$) or color-octet ($c = 8$) static quark-antiquark pair.

The ISR functions for the production of various initial-states and color-states up to NLO are given by

$$F_i^{(c)}(z) = \delta(1-z) + \frac{\alpha_s(\mu_F)}{\pi}\left[f_i^{(c)}\left(z, \frac{\mu_F}{2m_t}\right) + k_i^{(c)}\left(\frac{\mu_F}{2m_t}\right)\delta(1-z) + g_i^{(c)}\left(z, \frac{\mu_F}{2m_t}\right)\right]. \tag{4}$$

$f_i^{(c)}$ and $k_i^{(c)}$ express emissions of soft/collinear gluon, while $g_i^{(c)}$ express emissions of non-collinear gluon. Note, the latter term is neglected in ref. [9], but complemented in ref. [10] and the numerical size of the effect turns out to be non-negligible.

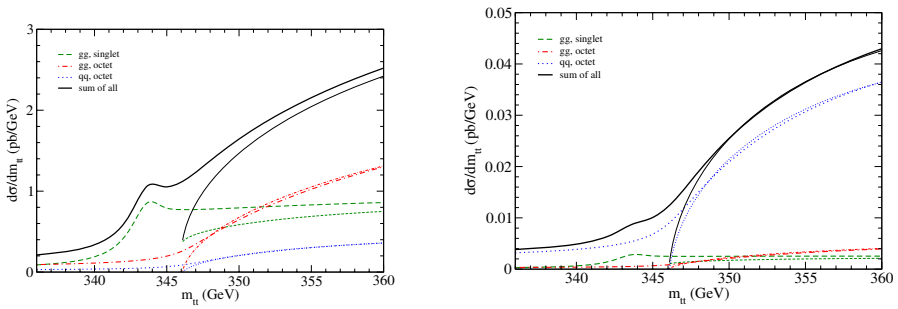

Fig. 1. – (Colour on-line) $t\bar{t}$ invariant-mass distributions in the threshold region at the LHC $\sqrt{s} = 14\,\text{TeV}$ (left) and at the Tevatron $\sqrt{s} = 1.96\,\text{TeV}$ (right). The color-singlet (green dashed) and octet (red dot-dashed) in gg channel, color-octet in $q\bar{q}$ channel (blue dotted), and the sum of them (black solid) are plotted. Thick lines include both bound-state and ISR effects, while thin lines represent the cross-sections with only NLO effects.

The hard correction factors are also known to NLO for various initial and color states;

$$K_i^{(c)} = 1 + \frac{\alpha_s(\mu_R)}{\pi} h_i^{(c)} \left(\frac{\mu_R}{m_t}\right). \tag{5}$$

Complete expressions of $h_i^{(c)}$ can be found in refs. [9, 10] where they are extracted from refs. [19, 20]; see also ref. [21].

Finally, the parton luminosity function is defined as

$$\frac{\mathrm{d}\mathcal{L}_i}{\mathrm{d}\tau}(\tau) = \sum_{\{a,b\}} \int \mathrm{d}x_1 \int \mathrm{d}x_2 f_a(x_1, \mu_F) f_b(x_2, \mu_F) \delta(\tau - x_1 x_2), \tag{6}$$

where the summation is over $\{a, b\} = \{g, g\}$ for $i = gg$, and $\{a, b\} = \{q, \bar{q}\}$, $\{\bar{q}, q\}$ with $q = u, d, c, s, b$ for $i = q\bar{q}$.

In fig. 1, we plot the $t\bar{t}$ invariant-mass distribution at the LHC $\sqrt{s} = 14\,\text{TeV}$ (left) and at the Tevatron (right), where we show explicitly the individual contributions from the gg color-singlet (dashed), gg color-octet (dot-dashed), and $q\bar{q}$ (dotted) channels, as well as the sum of them (solid). Thick lines include both bound-state and ISR effects, while thin lines include only the $\mathcal{O}(\alpha_s)$ corrections after expanding all the correction terms by α_s. For the numerical evaluation, we use the NLO potential [22] with the Bohr scale $\mu_B = 20\,\text{GeV}$, and CTEQ6M parton distribution functions [23] with $\mu_R = \mu_F = m_t$. At the LHC, the invariant-mass distribution for the sum of all channels still exhibits the $1S$ peak below the threshold, while it gradually approaches the NLO distribution above the threshold. The color-singlet gg channel dominates the cross-section below and near the $t\bar{t}$ threshold, while the color-octet gg channel is dominant above the threshold. On the other hand, at the Tevatron, due to the dominance of $q\bar{q}$ channel, bound-state effects are less significant.

Before closing this section, we comment on the difference between the results in [9] and in [10]. As we mentioned above, the regular terms in the ISR function are neglected

in [9], while complemented in [10]. These terms, however, are numerically sizable giving an additional enhancement on the magnitude of the ISR for each channel. Note, the ISR effects are rather uniform in the $m_{t\bar{t}}$ distribution, thus they act on the normalization of the cross-sections. Moreover, ref. [10] has examined the resummation of the threshold logarithms which further gives 10% level enhancement of the ISR effects. Note that, the resummation of both the Coulomb corrections and the threshold logarithms is formulated in ref. [14].

3. – Top-quark kinematical distributions

In this section, we briefly explain an inclusion of bound-state effects to the fully differential distributions in $t\bar{t}$ production at hadron colliders. The detail description can be found in ref. [11]. The method to incorporate bound-state effects to the fully differential cross-sections has been developed in e^+e^- collision [24,25], making use of the momentum-space Green's functions.

In contrast to the e^+e^- collision, at hadron colliders, the (partonic) collision energy is not fixed. Therefore, we have to set up a framework which is valid both in the threshold region ($m_{t\bar{t}} \simeq 2m_t$) and in the high-energy region ($m_{t\bar{t}} \gg 2m_t$). The former region is where the bound-state effects (Coulomb corrections) become significant and where the non-relativistic approximation is valid. On the other hand, in the latter region, the bound-state effects are not significant and the top quarks are relativistic. We present a framework which takes into account all the leading-order (LO) corrections in both regions. Namely, we incorporate all the $(\alpha_s/\beta)^n$ terms in the threshold region, while we include all the β^n terms in the relativistic region.

To take into account off-shellness of the top quarks, full amplitudes for the $bW^+\bar{b}W^-$ final-state have to be constructed. In the $bW^+\bar{b}W^-$ production, there are non-resonant diagrams where bW^+ and $\bar{b}W^-$ are not produced from the decay of t and $\bar{t}$, respectively. In the threshold region, either of t and $\bar{t}$ tends to be off-shell due to the restricted phase-space and the binding effects, and the non-resonant diagrams can give non-negligible contributions compared to the resonant diagrams. Since these contributions interfere with each other, all the diagrams have to be taken into account at the amplitude level. We divide the $bW^+\bar{b}W^-$ amplitudes into two parts, the $t\bar{t}$ (double-resonant) part and the remaining non-resonant part, as

$$\mathcal{M}^{(c)}_{bW^+\bar{b}W^-} = \mathcal{M}^{(c)}_{t\bar{t}} + \mathcal{M}^{(c)}_{\rm nr}. \tag{7}$$

In general each part is gauge dependent. We work in Feynman gauge for $SU(3)_{\rm c}$ and in unitary gauge for the broken electroweak symmetry. Furthermore, we employ the fixed-width scheme in the top-quark propagators.

The formula to incorporate bound-state effects in the resonant amplitudes is given by

$$\mathcal{M}^{(c)}_{t\bar{t}} = \mathcal{M}^{(c)}_{t\bar{t},\rm tree} \times \frac{G^{(c)}(E' + i\Gamma_t, \vec{p})}{G_0(E' + i\Gamma_t, \vec{p})}, \tag{8}$$

with $E' = E + E^2/(4m_t)$, and $E = m_{t\bar{t}} - 2m_t$. The momentum-space Green's functions are defined as

$$G^{(c)}(E + i\Gamma_t, \vec{p}) = \int \mathrm{d}^3\vec{r} e^{-i\vec{p}\cdot\vec{r}} \widetilde{G}^{(c)}(E + i\Gamma_t, \vec{r}). \tag{9}$$

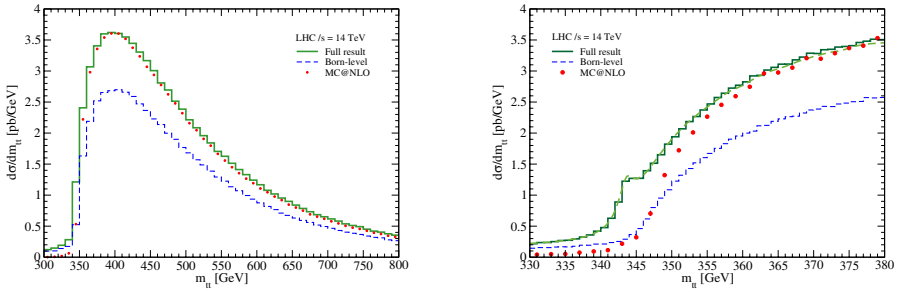

Fig. 2. – (Colour on-line) $t\bar{t}$ invariant-mass distribution in $pp \to bW^+\bar{b}W^-$ production at $\sqrt{s} =$ 14 TeV. Green solid line is the full cross-section and blue dashed line is the result in Born-level. The NLO $t\bar{t}$ production computed by using `MC@NLO` is also plotted in red dots.

The use of the modified energy E' in the formula turns out to be indispensable to extrapolate the Green's function formalism to the high-energy region. It is motivated by the fact that the Green's function, which dictates the time evolution of the $t\bar{t}$ system, is identified as a part of the Feynman amplitudes for $i \to t\bar{t} \to bW^+\bar{b}W^-$. The advantage of using $\widetilde{G}^{(c)}(E' + i\Gamma_t, \vec{p})$ is that one can obtain it from the conventional non-relativistic Green's function with a minimal modification $E \to E' = E + E^2/(4m_t)$.

Another aspect to be considered is the effects of large Γ_t. As an inevitable consequence of numerically integrating the fully differential cross-sections for $bW^+\bar{b}W^-$ final-state, there is a significant effect, known as the phase-space-suppression effect [24]. This suppression comes from the reduction of the phase-space of bW which decayed from the off-shell t or $\bar{t}$. However, a remarkable feature is known that Coulomb-enhancement effects due to the gluon exchange between t and $\bar{b}$ (decayed from $\bar{t}$) and between $\bar{t}$ and b cancel this effect [26]. The phase-space suppression effect is automatically incorporated, while the Coulomb-enhancement effect is difficult to incorporate in our numerical calculation. Thus, we multiply the $t\bar{t}$ amplitude $\mathcal{M}^{(c)}_{t\bar{t}}$ by an enhancement factor such that the phase-space-suppression factor is canceled. Since the cancellation is only guaranteed for the integrated cross-section at each $m_{t\bar{t}}$ [26], our prescription is only effective.

For the numerical calculation, we develop a Monte Carlo event-generator which implements the ingredients explained above([2]). The helicity amplitudes for $bW^+\bar{b}W^-$ resonant and non-resonant diagrams are calculated by using `HELAS` [27], based on the `MadGraph` [28] output. They are modified to implement the color-decomposition and to include the bound-state effects via the Green's functions. The phase-space integrations are performed by using `BASES/SPRING` [29], or alternatively by adapting our code to `MadEvent` [30, 31] (ver. 4.4.42). The ISR effects are partly incorporated by connecting our framework to parton-shower simulators. In addition, we include "K-factors" as the normalization constants of the cross-section for each individual channel. They are determined such that the $m_{t\bar{t}}$ distribution for each channel matches the corresponding NLO prediction in the threshold region.

In fig. 2 (left), we plot the $t\bar{t}$ invariant-mass distribution in $pp \to bW^+\bar{b}W^-$ production at $\sqrt{s} = 14$ TeV. The green solid line represents the full result which includes the

([2]) The Fortran code for the event generator including the bound-state correction is available at `http://madgraph.kek.jp/~yokoya/TopBS/`.

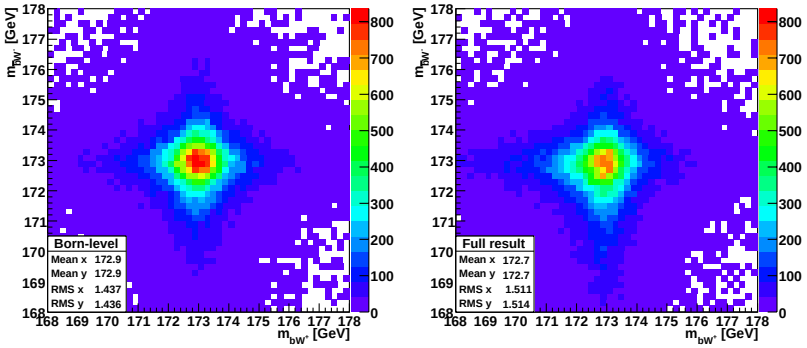

Fig. 3. – Two-dimensional distribution histogram in the bW^+ and $\bar{b}W^-$ invariant masses, for the events with $m_{t\bar{t}} \leq 370\,\text{GeV}$ at the LHC $\sqrt{s} = 14\,\text{TeV}$. Left figure is the Born-level prediction and right figure is the full result (including the Coulomb corrections and K-factors).

bound-state effects as well as the K-factors, and the blue dashed line represents the Born-level result (the LO prediction in the conventional perturbative QCD approach). Figure 2 (right) shows a magnification of the same cross-sections in the threshold region. As shown in fig. 1, theoretically the bound-state effects can be seen most clearly in the shape of the $m_{t\bar{t}}$ distribution in the threshold region [9,10]. Far above the threshold, the bound-state effects disappear and the cross-section approaches the Born-level distributions, up to the K-factor normalization.

In the same figures, we also compare our prediction with the NLO $m_{t\bar{t}}$ distribution computed by `MC@NLO` [32,33] with CTEQ6M PDFs and the scale choice of $\mu_F = \mu_R = \sqrt{m_t^2 + p_{T,t}^2}$. The latter prediction includes the full NLO QCD corrections for the on-shell $t\bar{t}$ productions. Below and near the threshold, our prediction is much larger than the `MC@NLO` prediction, due to the bound-state formation. The two cross-sections become approximately equal from around $m_{t\bar{t}} \sim 370$–$380\,\text{GeV}$ up to larger $m_{t\bar{t}}$.

One observes a characteristic bound-state effect in the (bW^+)-$(\bar{b}W^-)$ double-invariant-mass distribution. In fig. 3, we show the density plots of the invariant masses of the bW^+ and $\bar{b}W^-$ systems, given by a) the Born-level prediction and b) our full prediction. The Born-level prediction (a) is essentially determined by the product of the Breit-Wigner functions, hence the distribution is almost reflection symmetric with respect to the on-shell lines $(p_b + p_{W^+})^2 = m_t^2$ and $(p_{\bar{b}} + p_{W^-})^2 = m_t^2$. By contrast, the distribution by our full prediction (b) is not symmetric and biased towards the configuration, where one of t or $\bar{t}$ is on-shell and the other has an invariant-mass smaller than m_t.

4. – Discussions

In this section, we briefly discuss a prospect of using the threshold events for the study of the top-quark mass measurement at the LHC. Here, the threshold events may be defined as those with $|m_{t\bar{t}} - 2m_t| \simeq 10\,\text{GeV}$. As we have examined above, there can exist a significant bound-state effect even at hadron colliders.

The most attractive application of using the threshold events seems the precise determination of the top-quark mass (and ultimately the decay-width). Not only the direct

measurement of the broad resonance peak, but also the kinematical distributions of the decay products focusing on the threshold events have particular sensitivity to them. It is closely related with the mass definition of the heavy quarks. It has been pointed out that the *pole mass* of heavy quarks, defined as a location of the pole of the propagator, has a conceptual problem on its sensitivity to the exchange of infra-red gluons (IR renormalon). Moreover, theoretical predictions using the pole-mass scheme is known to show bad perturbative convergency. Solutions to this problem have been proposed, that is to use the so-called short-distance masses [7]. Since most of them are designed for the threshold production of $t\bar{t}$ bound-state at e^+e^- collider, they can be also applied for the threshold events at hadron colliders([3]). Indeed, the peak position as well as the shape of the $t\bar{t}$ resonance is less affected by the QCD ISR at hadron colliders, therefore, investigating the threshold events at the LHC can precede a future e^+e^- collider in time, although the accuracies to be reached are different.

However, at the LHC, systematical errors and also combinatorial ambiguities due to the undetectable neutrino(s) disturb the event-by-event $m_{t\bar{t}}$ determination. Since the threshold events occupy only a small fraction of the whole $t\bar{t}$ events $\sim 1\%$ or $\sim 10\,\mathrm{pb}$ at the LHC, therefore the large-$m_{t\bar{t}}$ events contribute as significant background. Thus, one needs to extract the threshold events in good accuracy. For the reduction of systematical errors, the most serious ingredient may be a jet-energy-scale. In this sense, di-lepton decay mode may be the most suitable channel for precisely determining $m_{t\bar{t}}$, even though 8-fold solutions must be resolved. This kind of measurement may be possible at the middle or latter stage of the LHC operation, after the detector performance for jet activities is well understood and several tens fb^{-1} of integrated luminosity is accumulated. Further careful analyses are required.

5. – Conclusions

In this contribution, we have reported recent studies on the bound-state effects in $t\bar{t}$ production at hadron colliders. The $t\bar{t}$ invariant-mass distribution as well as the top-quarks kinematical distributions very close to the threshold are calculated, including the all-order summation of Coulomb singularities which causes a formation of a broad resonance using the non-relativistic QCD framework and also the effects of ISR which enhance the cross-sections significantly but rather uniformly in $m_{t\bar{t}}$.

The threshold events contain rich information for the determination of the top-quark mass in the short-distance mass scheme which is therefore free from IR-renormalon ambiguity and has good perturbative convergency. A precise determination of $m_{t\bar{t}}$ to several GeV level needs to reduce the systematical errors drastically, and to reduce combinatorial ambiguities to avoid background contributions from the large-$m_{t\bar{t}}$ events. Furthermore, to find observables which are sensitive to the mass and rather free from the experimental ambiguities, is our future progress.

* * *

I thank K. Hagiwara and Y. Sumino for collaboration on the works presented here. I also thank the organizers for the invitation, and especially F. Maltoni for encouraging comments and discussions.

([3]) We note that a first attempt to extract another short-distance mass, the $\overline{\mathrm{MS}}$ mass, from the total cross-section measurement at the Tevatron is performed in ref. [34].

REFERENCES

[1] Tevatron Electroweak Working Group and CDF Collaboration and D0 Collaboration, arXiv:0903.2503 [hep-ex].
[2] Datta M., these proceedings.
[3] Harel A., these proceedings.
[4] Bigi I. I. Y., Dokshitzer Y. L., Khoze V. A., Kuhn J. H. and Zerwas P. M., *Phys. Lett. B*, **181** (1986) 157.
[5] Fadin V. S. and Khoze V. A., *JETP Lett.*, **46** (1987) 525; *Pisma Zh. Eksp. Teor. Fiz.*, **46** (1987) 417.
[6] Fadin V. S. and Khoze V. A., *Sov. J. Nucl. Phys.*, **48** (1988) 309; *Yad. Fiz.*, **48** (1988) 487.
[7] Hoang A. H. *et al.*, *Eur. Phys. J. direct C*, **2** (2000) 1, and references therein.
[8] Fadin V. S., Khoze V. A. and Sjostrand T., *Z. Phys. C*, **48** (1990) 613.
[9] Hagiwara K., Sumino Y. and Yokoya H., *Phys. Lett. B*, **666** (2008) 71.
[10] Kiyo Y., Kuhn J. H., Moch S., Steinhauser M. and Uwer P., *Eur. Phys. J. C*, **60** (2009) 375.
[11] Sumino Y. and Yokoya H., *JHEP*, **1009** (2010) 034.
[12] Kim C. and Mehen T., *Phys. Rev. D*, **79** (2009) 035011.
[13] Hagiwara K. and Yokoya H., *JHEP*, **0910** (2009) 049.
[14] Beneke M., Falgari P. and Schwinn C., *Nucl. Phys. B*, **828** (2010) 69.
[15] Kauth M. R., Kuhn J. H., Marquard P. and Steinhauser M., *Nucl. Phys. B*, **831** (2010) 285.
[16] Kats Y. and Schwartz M. D., *JHEP*, **1004** (2010) 016.
[17] Younkin J. E. and Martin S. P., *Phys. Rev. D*, **81** (2010) 055006.
[18] Idilbi A., Kim C. and Mehen T., arXiv:1007.0865 [hep-ph].
[19] Kuhn J. H. and Mirkes E., *Phys. Rev. D*, **48** (1993) 179.
[20] Petrelli A., Cacciari M., Greco M., Maltoni F. and Mangano M. L., *Nucl. Phys. B*, **514** (1998) 245.
[21] Czakon M. and Mitov A., *Nucl. Phys. B*, **824** (2010) 111.
[22] Kniehl B. A., Penin A. A., Schroder Y., Smirnov V. A. and Steinhauser M., *Phys. Lett. B*, **607** (2005) 96.
[23] Pumplin J., Stump D. R., Huston J., Lai H. L., Nadolsky P. and Tung W. K., *JHEP*, **0207** (2002) 012.
[24] Sumino Y., Fujii K., Hagiwara K., Murayama H. and Ng C. K., *Phys. Rev. D*, **47** (1993) 56.
[25] Jezabek M., Kuhn J. H. and Teubner T., *Z. Phys. C*, **56** (1992) 653.
[26] Modritsch W. and Kummer W., *Nucl. Phys. B*, **430** (1994) 3.
[27] Murayama H., Watanabe I. and Hagiwara K., KEK-91-11.
[28] Stelzer T. and Long W. F., *Comput. Phys. Commun.*, **81** (1994) 357.
[29] Kawabata S., *Comput. Phys. Commun.*, **41** (1986) 127.
[30] Maltoni F. and Stelzer T., *JHEP*, **0302** (2003) 027.
[31] Alwall J. *et al.*, *JHEP*, **0709** (2007) 028.
[32] Frixione S. and Webber B. R., *JHEP*, **0206** (2002) 029.
[33] Frixione S., Nason P. and Webber B. R., *JHEP*, **0308** (2003) 007.
[34] Langenfeld U., Moch S. and Uwer P., *Phys. Rev. D*, **80** (2009) 054009.